Journal of Catalysis 397 (2021) 233–244

Contents lists available at ScienceDirect

Journal of Catalysis

journal homepage: www.elsevier.com/locate/jcat

Predicting macro-kinetic observables in electrocatalysis using the generalized degree of rate control

Adam Baz, Adam Holewinski *

Department of Chemical and Biological Engineering, University of Colorado Boulder, Boulder, CO 80309, United States
Renewable and Sustainable Energy Institute, University of Colorado Boulder, Boulder, CO 80309, United States

ARTICLE INFO

Article history:
Received 10 January 2021
Revised 1 March 2021
Accepted 8 March 2021
Available online 18 March 2021

Keywords:
Degree of rate control
Tafel slope
Transfer coefficient
Apparent activation energy
Microkinetic model
Electrocatalysis

ABSTRACT

Kinetic observables such as the Tafel slope, apparent activation energy, and apparent reaction orders all provide mechanistic fingerprints for electrocatalytic processes. Here, we show how each of these quantities is related to the generalized degree of rate control (DRC). We find that the apparent transfer coefficient, an inverted form of the Tafel slope, is a weighted average of the number of electrons transferred to generate each intermediate or product species in a mechanism, where the weighting factor is the DRC. We similarly show that the apparent activation energy and apparent reaction orders (with potential dependence) can also be written in simple terms of the DRC. Since DRCs can further be related with microscopic quantities such as fractional coverages of intermediates, these relations can be used to improve intuition about possible operative mechanisms of complex electrocatalytic processes. Final discussions address the possible impacts of various nonidealities such as electric field effects, adsorbate interactions, and approximations related to the form of electrochemical rate constants.

1. Introduction

The Tafel slope, apparent reaction order, and apparent activation energy describe how the rate of reaction is affected by changes to the applied potential, reactant/product concentration, and temperature, respectively. While apparent reaction orders and activation energies are common to both electrochemical and thermal reactions, the Tafel slope is unique to electrochemistry. When the reaction is far from equilibrium, the Tafel slope is generally defined by a linear phenomenological relationship between applied potential and logarithmic current density:

$$\eta = a + b\log(i) \tag{1}$$

where η is the applied overpotential ($\eta = E - E_{EQ}$ where E is the applied potential and E_{EQ} is the equilibrium potential), i is the current density, a is a constant related to the (extrapolated) exchange current density at equilibrium, and b is the Tafel slope [1]. This relationship describes the empirical observation that the current density of electrochemical reactions at large overpotential tends to increase exponentially with the applied potential, absent ohmic or mass-transport related losses. For electrocatalytic reactions, which are typically characterized by complex mechanisms involving a number of adsorbed intermediates on the surface of the electrode/catalyst, the rate is not always a simple exponential function of the potential, nor is the Tafel slope a constant as the applied potential changes [2,3]. As highlighted by previous works, the Tafel slope relates to various characteristics of a reaction, such as the coverages of adsorbates, their isotherms, and the identity of the rate-determining step(s) (RDS), all of which may be potential-dependent [4–7]. If these factors are taken into account through microkinetic modeling, then the Tafel slope can provide insight into the mechanism of an electrocatalytic process [8–11]. While the Tafel slope is typically reported in units of mV/dec, this information is more usefully compared in microkinetic models by way of its inverted form, the apparent transfer coefficient [12,13]. For an electrochemical process operating far from equilibrium, the apparent transfer coefficient can be written as:

$$\alpha = \frac{RT}{F}\frac{\partial \ln|i|}{\partial E} \tag{2}$$

where R is the ideal gas constant, T is the temperature, and F is the Faraday constant. Accordingly, the Tafel slope and the apparent transfer coefficient are related by:

$$b = \frac{\partial E}{\partial \log|i|} = \frac{2.3RT}{\alpha F} \tag{3}$$

While the apparent transfer coefficient is similar to both the apparent activation energy and apparent reaction order in that it

* Corresponding author at: University of Colorado, 27 UCB, Suite N332, SEEC, Boulder, CO 80309, United States.
E-mail address: adam.holewinski@colorado.edu (A. Holewinski).

https://doi.org/10.1016/j.jcat.2021.03.014
0021-9517/

is experimentally observable, its connection to the degree of rate control concept has not been developed. Campbell's generalized degree of rate control (DRC) is a sensitivity analysis that describes how the rate of reaction toward a given product is affected by a small perturbation to the standard-state Gibbs free energy (G^0) of a given species (including intermediates, transition states, and products) in the kinetic pathway, holding all other standard-state Gibbs free energies constant [14,15]. Relationships have been identified between the apparent activation energy and the degree of rate control, but to the best of our knowledge, similar connections have not been made for the apparent transfer coefficient [16,17]. Formally, the DRC is written as:

$$X_i = \left.\frac{\partial \ln(r)}{\partial\left(-G_i^0/RT\right)}\right|_{G^o_{j\neq i}} \tag{4}$$

where G_i^0 is the standard-state Gibbs free energy of the i^{th} species in the mechanism (referenced relative to the standard-state stoichiometrically-combined reactants), and $G^0_{j\neq i}$ indicates that the standard-state Gibbs free energies of all other species are held constant. In other words, the DRC is a measure of the change in the magnitude of the rate of reaction per RT decrease in the standard-state Gibbs free energy of a given species. A positive value indicates that stabilizing the species would result in an increase in the rate, while a negative value indicates that destabilizing the species would increase the rate. The sum of all transition state DRCs has been proven to be equal to 1 [18]), while stable adsorbed intermediates exhibit DRCs that are related to their fractional site coverage and typically take on negative values (i.e inhibition) [19]. Naturally, a DRC of 0 indicates that the energy of the species does not affect the rate (i.e for transition states the corresponding elementary step is "fast", and for stable intermediates the extent of rate inhibition is minimal).

Recently, Mao and Campbell derived a general equation for the apparent activation energy of arbitrary reaction mechanisms. They found that the apparent activation energy can be written as RT plus a weighted average of the standard-state enthalpies of all intermediates (including transition states and products), where the weighting factor is the DRC [17]. In this work, we extend the concept to electrochemistry, first via expressions for the apparent transfer coefficient of a general electrocatalytic mechanism. The resultant equation takes a similar form to that for the apparent activation energy: the apparent transfer coefficient equals the weighted number of electrons transferred (relative to the reactants) to reach each intermediate or product species, where the weighting factor is the DRC of the respective species. Additionally, we provide derivations for the apparent reaction order and the apparent activation energy in terms of the DRC for a generalized electrocatalytic mechanism. We first present the derivations, then provide examples showing the validity of the equations for several electrocatalytic mechanisms. Finally, we discuss the possible impacts of various nonidealities such as electric field effects, adsorbate interactions, and approximations related to the form of electrochemical rate constants, as well as implications toward improved mechanistic insight for electrochemical reactions.

2. Derivations

2.1. Apparent transfer coefficient

As previously stated by others [17], the total rate of a composite reaction can be written within transition state theory as the product of two contributions (for convenience in notation, we will work with the reduced standard Gibbs free energy: $g_i = -G_i^0/RT$):

$$r = \frac{k_B T}{h} \times f(g_1, g_2, \cdots, g_N, a_1, a_2, \cdots, a_M) \tag{5}$$

where the second term is a general function, f, which depends on the standard-state Gibbs free energies of all species (including intermediates, products, and transition states) as well as the activities of all fluid-phase reactant/product species. Here, the g_i terms define the rate and equilibrium constants of all elementary steps. By plugging this rate term into the definition of the apparent transfer coefficient (and noting that the current density of an electrochemical process is proportional to the rate of reaction) one may write:

$$\alpha = \frac{RT}{F}\left[\frac{\partial \ln\left(\frac{k_B T}{h}\right)}{\partial E} + \frac{\partial \ln(f)}{\partial E}\right] \tag{6}$$

where the first term disappears since it has no dependence on the potential. One may then apply the chain rule to the second term to separate out the explicit dependence of each g_i on the applied potential:

$$\alpha = \frac{RT}{F}\left[\sum_i \frac{\partial \ln(f)}{\partial g_i}\frac{\partial g_i}{\partial E}\right] \tag{7}$$

where a summation is run over all of the intermediates, transition states, and products. The first term inside the summation is equivalent to the DRC, which allows us to write:

$$\alpha = \frac{RT}{F}\left[\sum_i X_i \frac{\partial g_i}{\partial E}\right] = \frac{RT}{F}\left[\sum_i X_i \frac{\partial(-G_i^0/RT)}{\partial E}\right] \tag{8}$$

In electrochemical mechanisms, the formation of various intermediates is associated with the transfer of some number of electrons either into (oxidation) or out of (reduction) the electrode. The standard-state Gibbs free energy of species "i" with n_i electrons transferred to produce that species (relative to the reactants) can be written as follows:

$$G_i^0 = G_{i,ref}^0 + \left(H_i^0 - H_{i,ref}^0\right) - T\left(S_i^0 - S_{i,ref}^0\right) - n_i F(E - E_{ref}) \tag{9}$$

Here, E_{ref} is an arbitrary reference potential, while $H^0_{i,ref}$ and $S^0_{i,ref}$ are the standard-state enthalpy and entropy, respectively, of the species i evaluated at the reference potential. It can be convenient to set E_{ref} equal to a standard reference electrode potential or the equilibrium potential of the overall reaction, but ultimately the choice is arbitrary. H_i^0 and S_i^0 represent the standard-state enthalpy and entropy of species i at the operating potential, E. In this formulation, electrons are not explicitly counted among the i species, but rather they are associated with a given species as the number transferred (relative to the reactant state) to yield that species; their energy deviations from the reference potential are accounted solely by the potential energy contribution in the final term. We will first assume that the standard enthalpies and entropies of chemical species do not change with potential (nonidealities such as electric field effects on chemical adsorbates will be considered in *Section 3.4*) such that the only contribution to the potential dependence of G_i^0 is due to the free energy of the n_i electrons associated with the formation of species i. Therefore, $\Delta H_i^0 = \Delta S_i^0 = 0$ leaving the expression:

$$G_i^0 = H_{i,ref}^0 - TS_{i,ref}^0 - n_i F(E - E_{ref}) \tag{10}$$

It is important to note that reaction intermediates, products, *and* transition states are all counted among the i species. This can be interpreted in a Butler-Volmer framework, where the electrochemical symmetry factor, β_i, can be effectively considered an extent of partial charge transfer between the reactant and

transition state of a given elementary electron transfer step [20–22]. Therefore, n_i for intermediates will be an integer value, while for transition states it may contain fractional contributions. There is also an implicit assumption here that the symmetry factor does not change as a function of potential. This is generally a sufficient approximation as β_i values usually vary slowly over wide potential windows, and they will be essentially constant when considering the small perturbation of potential to get a local transfer coefficient at any given potential [23]. Deviations such as those captured in Marcus theory are discussed in *Section 3.4*. Using the aforementioned framework, the apparent transfer coefficient can then be written as:

$$\alpha = \frac{RT}{F}\left[\sum_i X_i \frac{\partial\left[\frac{-H^0_{i,ref}}{RT} + \frac{S^0_{i,ref}}{R} + \frac{n_i F(E-E_{ref})}{RT}\right]}{\partial E}\right] \tag{11}$$

which reduces to:

$$\alpha = \sum_i X_i n_i \tag{12}$$

Therefore, for "ideal" cases where the potential only affects the free energy of the electrons associated with the formation of a given species, the apparent transfer coefficient is the sum of the number of electrons associated with each species, weighted by the respective DRC of that species.

2.2. Apparent activation energy

The apparent activation energy describes how the rate of reaction changes given a change in the temperature and can be formally written as the following:

$$E_{app} = -R\left[\frac{\partial \ln(r)}{\partial(1/T)}\right] = RT^2\left[\frac{\partial \ln(r)}{\partial(T)}\right] \tag{13}$$

Campbell and Mao previously provided a comprehensive derivation of the apparent activation energy in terms of the DRC for a general reaction mechanism [17]. Taking the same approach as above but using the appropriate temperature derivative, this reduces to:

$$E_{app} = RT + \sum_i X_i H^0_i \tag{14}$$

To show the potential dependence of their equation in an electrocatalytic mechanism, we separate the free energy of n_i electrons associated with the i^{th} species, keeping the same "ideal" conditions as described in Section 2.1:

$$E_{app} = RT + \sum_i X_i\left[G^0_i + TS^0_{i,ref}\right] \tag{15}$$

Converting back to molecular units and simplifying:

$$E_{app} = k_B T + \sum_i X_i\left[H^0_{i,ref} - n_i(E - E_{ref})\right] \tag{16}$$

Recognizing that the apparent transfer coefficient can be written as $\sum_i X_i n_i$, we identify a direct relationship between the apparent activation energy and the apparent transfer coefficient, written as:

$$E_{app} = k_B T + \left[\sum_i X_i H^0_{i,ref}\right] - \alpha(E - E_{ref}) \tag{17}$$

The diagnostic use remains the same as always in terms of finding consistency between an apparent activation energy and mechanism, though some additional corroboration may be gained by determining the apparent activation energy at variable potential.

2.3. Apparent reaction order

Evaluation of the apparent reaction order (δ_i) involves varying the thermodynamic activity of the fluid-phase reactants or products and observing the resulting change in the rate of reaction (current):

$$\delta_i = \frac{\partial \ln|i|}{\partial \ln(a_i)} \tag{18}$$

where a_i is the activity of species *i*. Practically, this involves varying the fluid-phase species' pressure or concentration, and we will only consider the case of ideal gases and ideal solutions, where the distinction with activity is inconsequential. A change in a fluid-phase species' activity produces a change in its Gibbs free energy:

$$G_i = G^0_i + k_B T \ln a_i \tag{19}$$

Thus, changing the reduced standard-state Gibbs free energy, $\frac{G^0_i}{k_B T}$, by one unit has the same impact on the overall free energy of a species as changing the activity by one unit of $\ln(a_i)$. However, considering Eqs. (18) and (19) in relation to the DRC raises two mild predicaments: first, the DRC is defined with respect to perturbing the standard state, as given in Eq. (4), rather than perturbing the activity; second, the zero-energy reference state is normally taken to be the stoichiometrically-combined reactants at the standard state, requiring consideration of the consequences of a shifting reference system.

The analysis is simplest for intermediate or product species, which are already counted among the *i* species in a DRC analysis and do not affect the reference state. Here we can recognize that, within transition state theory, every elementary rate term (forward or reverse) is derived from an equilibrium between the initial and transition states, and thus has the form:

$$r_n \propto a_i^{\nu_i}\prod_{j\neq i} a_j^{\nu_j}\exp\left(g^{0,\ddagger}_{TS} - \nu_i g^0_i - \Sigma\nu_{j\neq i} g^0_{j\neq i}\right) \tag{20}$$

where ν_i is the stoichiometric coefficient of species *i* in the elementary step *n*. In this case, perturbing the reduced standard-state Gibbs free energy and perturbing the natural logarithm of the activity have the same magnitude of impact on the rate:

$$\left.\frac{\partial \ln(r)}{\partial\left(-G^0_i/k_B T\right)}\right|_{G^0_{j\neq i}} = -\frac{\partial \ln(r)}{\partial \ln a_i} \tag{21}$$

Since every term in a system of coupled rates will be influenced to the same degree by the two modes of perturbation, it can be expected that the system as a whole will react identically and Eq. (21) is general. The effects could also be illustrated to propagate term-wise through closed-form composite rate laws. Thus the DRC for fluid-phase intermediate and product species can be seen as equivalent to the negative apparent reaction order, which has been identified by others [18,19]:

$$X_i = -\delta_i \tag{22}$$

The apparent reaction order with respect to reactant species must be treated differently, since the stoichiometrically-combined reactants are considered as the zero-energy reference state. If we were to consider the free energy of all species relative to an absolute reference state, perturbing a reactant's activity would be no different than for a product, and we would arrive again at Eq. (22). If the reactant state is "re-zeroed" after the perturbation of an activity, we can view this as an effective perturbation on all the other states relative to a fixed point representing the

reactants. Each species' free energy undergoes an apparent move to a value (noted as G_i') in accordance with the changes in moles of reactant to form that species:

$$G_i^{'} = H_{i,ref}^0 - TS_{i,ref}^0 + \left(v_{j\in G_{f,i}^0}\right)k_B T \ln a_j - n_i F\left(E - E_{ref}\right) \tag{23}$$

where $v_{j\in G_{f,i}^0}$ is the stoichiometric coefficient of reactant j (negative by convention) appearing in the formation energy of intermediate or product species i. In some works, this is also framed in terms of adjusting the reference energies of a linearly-independent basis set, conveniently chosen as all atomic species present in the mechanism [24]. A shift in the energy of the reactants (i.e. a shift in the reference) produces a commensurate shift in the energies of all species in the mechanism containing atomic species whose energies were defined by that reference. A detailed example of this is shown in the **Supporting Information**.

To define an apparent reactant order in the shifting reference basis, we follow the same approach as was taken for the apparent transfer coefficient and activation energy. We separate the rate into its contributions from the frequency factor and the function f which contains the standard-state Gibbs free energies and activities of each of the species in the mechanism:

$$\delta_j = \frac{\partial \ln\left(\frac{k_B T}{h}\right)}{\partial \ln(a_j)} + \frac{\partial \ln(f)}{\partial \ln(a_j)} \tag{24}$$

The frequency factor is independent of the activity, and the second term can be expanded in terms of apparent shifts in the free energies of the species in the mechanism. We note that it is arbitrary whether we assign the perturbations in free energy as an apparent change in each species' standard-state Gibbs free energy (mirroring the approach of previous sections) or if we take Eq. (23) to suggest apparent changes in activity due to the form of the term $\left(v_{j\in G_{f,i}^0}\right)k_B T \ln a_j$. These are mathematically equivalent assignments, per Eq. (21). We frame the expansion in terms of apparent activities (a_i') so that the reaction order becomes:

$$\delta_j = \sum_i \frac{\partial \ln(f)}{\partial \ln a_i'} \frac{\partial \ln a_i'}{\partial \ln a_j} \tag{25}$$

Eq. (23) then identifies the second term of each product as the reactant stoichiometric factor:

$$\frac{\partial \ln a_i'}{\partial \ln a_j} = v_{j\in G_{f,i}^0} \tag{26}$$

Combining with the equivalence between orders and DRC found in Eq. (22) we arrive at:

$$\delta_j = -\sum_i \left(v_{j\in G_{f,i}^0}\right) X_i \tag{27}$$

Therefore, the apparent reaction order of the j^{th} reactant species is the negative of the summation of the DRCs of each of the species in the pathway, multiplied by the reactant stoichiometric coefficient in the formation of the species.

3. Results and discussion

In this section we first provide analytical examples of the apparent transfer coefficient and reaction orders for sample mechanisms calculated explicitly, and with the DRC expressions derived in this work. Apparent activation energies are not analytically derived as they are merely application of formulas derived in other works, but analysis of activation energies will be shown in comparing with full numerical analyses later in the section. We close with discussion of "secondary" potential effects that can impact the measured kinetic parameters, such as electric field effects and adsorbate–adsorbate interactions.

3.1. Two-step mechanism with quasi-equilibrium – Analytical solution

We first consider the following generalized two-step mechanism (to be referred to as Mechanism 1), producing oxidized species O from reduced form R via adsorbed intermediate I^* (overall reaction $R \leftrightarrow O + 2e^-$):

$$R + (*) \leftrightarrow I^* + e^- \tag{M1.1}$$

$$I^* \leftrightarrow O + e^- + (*) \tag{M1.2}$$

Step (M1.1) is assumed to be quasi-equilibrated, with step (M1.2) being an irreversible rate-determining step, allowing one to write the following rate law (assuming a Langmuir adsorption isotherm):

$$r = k_2\theta_I = \frac{k_2 K_1 a_R}{1 + K_1 a_R} \tag{28}$$

Above, θ_I is the surface coverage of I^*, and the Butler-Volmer rate constant for an activated electrochemical elementary step may be written as:

$$k_2 = \frac{k_B T}{h}\exp\left(\frac{-\left(\Delta G_{ref,2}^{0,\ddagger} - \beta_2 F\left(E - E_{ref}\right)\right)}{RT}\right) \tag{29}$$

where $\Delta G_{ref,2}^{0,\ddagger}$ is the standard-state Gibbs free energy of activation at the reference potential E_{ref}, β_2 is the electrochemical symmetry factor for elementary step 2, and the other terms have their usual meaning. This can also be written in terms of the standard state Gibbs free energies of the intermediates and transition states in the mechanism as:

$$k_2 = \frac{k_B T}{h}\exp\left(\frac{-\left(G_{ref,TS,2}^0 - G_{ref,I}^0\right)}{RT}\right)\exp\left(\frac{\beta_2 F\left(E - E_{ref}\right)}{RT}\right) \tag{30}$$

where $G_{ref,i}^0$ is the standard state Gibbs free energy of intermediate i at the reference potential E_{ref}. This can be further simplified as:

$$k_2 = \frac{k_B T}{h}\exp\left(g_{ref,TS,2}\right)\exp\left(-g_{ref,I}\right)\exp\left(\frac{\beta_2 F\left(E - E_{ref}\right)}{RT}\right) \tag{31}$$

where it may be noted that the even more compact expression $\frac{k_B T}{h}\exp\left(g_{TS,2}\right)\exp\left(g_I\right)$ could be written, but it is more illustrative to keep the potential dependence explicitly shown. The equilibrium constant can also be written similarly:

$$\begin{aligned} K_1 &= \exp\left(\frac{-\left(\Delta G_{ref,1}^0 - F\left(E - E_{ref}\right)\right)}{RT}\right) \\ &= \exp\left(\frac{-\left(G_{ref,I}^0 - G_{ref,R}^0\right)}{RT}\right)\exp\left(\frac{F\left(E - E_{ref}\right)}{RT}\right) \\ &= \exp(g_{ref,I})\exp\left(\frac{F\left(E - E_{ref}\right)}{RT}\right) \end{aligned} \tag{32}$$

Plugging into the rate law gives:

$$r = \frac{\frac{k_B T}{h}\exp\left(g_{ref,TS,2}\right)\exp\left(\frac{\beta_2 F\left(E - E_{ref}\right)}{RT}\right)a_R\exp\left(\frac{F\left(E - E_{ref}\right)}{RT}\right)}{1 + \exp(g_{ref,I})\exp\left(\frac{F\left(E - E_{ref}\right)}{RT}\right)a_R} \tag{33}$$

The apparent transfer coefficient can then be evaluated as:

$$\alpha = \frac{RT}{F}\frac{\partial \ln(r)}{\partial E} = \frac{RT}{F}\left[\frac{\beta_2 F}{RT} + \frac{F}{RT} - \frac{F}{RT}\left[\frac{\exp\left(g_{ref,I}\right) a_R \exp\left(\frac{F\left(E-E_{ref}\right)}{RT}\right)}{1+\exp(g_{ref,I})\exp\left(\frac{F\left(E-E_{ref}\right)}{RT}\right)a_R}\right]\right] = \beta_2 + 1 - \theta_I \quad (34)$$

We may similarly evaluate the apparent reaction order with respect to a_R:

$$\delta_R = \frac{\partial \ln(r)}{\partial \ln\left(a_R\right)} = 1 - \theta_I \quad (35)$$

We now show that one can arrive at the same expressions by using the DRC equations identified in this work. The DRC of each intermediate species can be written as:

$$X_I = \frac{\partial \ln(r)}{\partial (g_I)} = \frac{\partial \ln(r)}{\partial \left(g_{ref,I}\right)} = -\left[\frac{\exp\left(g_{ref,I}\right)\exp\left(\frac{F\left(E-E_{ref}\right)}{RT}\right)a_R}{1+\exp\left(g_{ref,I}\right)\exp\left(\frac{F\left(E-E_{ref}\right)}{RT}\right)a^R}\right] = -\theta_I \quad (36)$$

$$X_{TS,2} = \frac{\partial \ln(r)}{\partial \left(g_{TS,2}\right)} = \frac{\partial \ln\left(r\right)}{\partial \left(g_{ref,TS,2}\right)} = 1 \quad (37)$$

while the DRC terms for the other species in the mechanism are equal to 0. Above, we have noted that $\frac{\partial \ln(r)}{\partial \left(g_{ref,i}\right)} = \frac{\partial \ln(r)}{\partial (g_i)}$ since $\frac{\partial (g_i)}{\partial \left(g_{ref,i}\right)} = 1$ and it is desirable to keep the rate law in the same form as previously for illustration. Plugging these terms into the equation for the apparent transfer coefficient yields:

$$\alpha = \sum_i X_i n_i = (X_I)(n_I) + (X_{TS,2})(n_{TS,2}) = (-\theta_I)(1) + (1)(1+\beta_2) = \beta_2 + 1 - \theta_I \quad (38)$$

which is identical to what was evaluated explicitly above. Similarly for the apparent reaction order:

$$\delta_R = -\sum_i \left(\nu_{j\in G^0_{f,i}}\right) X_i = -[(-1)(X_I) + (-1)(X_{TS,2})] = (-\theta_I) + (1) = 1 - \theta_I \quad (39)$$

which is also identical to that evaluated explicitly from the rate law above. We note that in this mechanism where arbitrary reactant species *R*, *I*, and *O* are used, the reactant stoichiometric coefficients are the trivial case of −1 for all species. Examples where maintaining atomic balance is required are outlined in *Section 3.3* and the **Supporting Information**.

We now consider the scenario for the same oxidation mechanism, but instead with step (M1.1) as the irreversible RDS, and step (M1.2) assumed to be quasi-equilibrated. The rate law can be written as:

$$r = \frac{k_1 K_2 a_R}{K_2 + a_O} \quad (40)$$

Plugging Butler-Volmer and Nernst equations in for the rate and equilibrium constants in the rate law gives:

$$r = \frac{\frac{k_B T}{h}\exp\left(g_{ref,TS,1}\right)\exp\left(\frac{\beta_1 F\left(E-E_{ref}\right)}{RT}\right)\exp\left(g_{ref,O}\right)\exp\left(-g_{ref,I}\right)\exp\left(\frac{F\left(E-E_{ref}\right)}{RT}\right)a_R}{\exp\left(g_{ref,O}\right)\exp\left(-g_{ref,I}\right)\exp\left(\frac{F\left(E-E_{ref}\right)}{RT}\right)+a_O} \quad (41)$$

which allows the apparent transfer coefficient to be written as:

$$\alpha = \frac{RT}{F}\frac{\partial \ln(r)}{\partial E} = \frac{RT}{F}\left[\frac{\beta_1 F}{RT} + \frac{F}{RT} - \frac{F}{RT}\left[\frac{\exp\left(g_{ref,O}\right)\exp\left(-g_{ref,I}\right)\exp\left(\frac{F\left(E-E_{ref}\right)}{RT}\right)}{\exp\left(g_{ref,O}\right)\exp\left(-g_{ref,I}\right)\exp\left(\frac{F\left(E-E_{ref}\right)}{RT}\right)+a_O}\right]\right] = \beta_1 + 1 - (1-\theta_I) = \beta_1 + \theta_I \quad (42)$$

The apparent reaction order can be similarly evaluated as:

$$\delta_R = \frac{\partial \ln(r)}{\partial \ln\left(a_R\right)} = 1 \quad (43)$$

The generalized DRCs for each of the species are:

$$X_I = \frac{\partial \ln(r)}{\partial (g_I)} = \frac{\partial \ln(r)}{\partial \left(g_{ref,I}\right)} = -1 - \left(-\frac{\exp\left(g_{ref,O}\right)\exp\left(-g_{ref,I}\right)\exp\left(\frac{F\left(E-E_{ref}\right)}{RT}\right)}{\exp\left(g_{ref,O}\right)\exp\left(-g_{ref,I}\right)\exp\left(\frac{F\left(E-E_{ref}\right)}{RT}\right)+a_O}\right) = -1 + (1-\theta_I) = -\theta_I \quad (44)$$

$$X_O = \frac{\partial \ln(r)}{\partial (g_O)} = \frac{\partial \ln\left(r\right)}{\partial \left(g_{ref,O}\right)} = 1 - \left(\frac{\exp\left(g_{ref,O}\right)\exp\left(-g_{ref,I}\right)\exp\left(\frac{F\left(E-E_{ref}\right)}{RT}\right)}{\exp\left(g_{ref,O}\right)\exp\left(-g_{ref,I}\right)\exp\left(\frac{F\left(E-E_{ref}\right)}{RT}\right)+a_O}\right) = 1 - (1-\theta_I) = \theta_I \quad (45)$$

$$X_{TS,1} = \frac{\partial \ln(r)}{\partial \left(g_{TS,1}\right)} = \frac{\partial \ln(r)}{\partial \left(g_{ref,TS,1}\right)} = 1 \quad (46)$$

while the DRC terms for the other species in the mechanism are equal to 0. Applying the equation for the apparent transfer coefficient:

$$\alpha = \sum_i X_i n_i = (X_I)(n_I) + (X_O)(n_O) + (X_{TS,1})(n_{TS,1}) = (-\theta_I)(1) + (\theta_I)(2) + (1)(\beta_1) = \beta_1 + \theta_I \quad (47)$$

which is identical to the result found explicitly above. Applying Eq. (27) for the apparent reaction order we also find:

$$\delta_R = -\sum_i \left(\nu_{j\in G^0_{f,i}}\right) X_i = -[(-1)(X_I) + (-1)(X_{TS,1}) + (-1)(X_O)] = (-\theta_I) + (1) + (\theta_I) = 1 \quad (49)$$

which is identical to that calculated explicitly above.

3.2. Two-step mechanism with no RDS assumption

In the preceding example, we solved for the apparent transfer coefficient, apparent reaction orders, and generalized degrees of rate control analytically, which was made easier by assuming one RDS with the other step quasi-equilibrated. For more complicated mechanisms, it is usually not possible to write analytical expressions for the rate law and kinetic quantities of interest, instead requiring solution of the full microkinetic model numerically (although in some cases, techniques such as analysis of maximum rates can be used to circumvent this) [25,26]. One can then perform a sensitivity analysis on the standard-state Gibbs free energies of each of the intermediates, transition states, and products to measure the DRC of each state. Similarly, one may

numerically calculate the steady-state rate of reaction at a series of different applied potentials, temperatures, and reactant/product activities to measure the apparent transfer coefficient, activation energy, and reaction orders, respectively. In this example, we solve the full microkinetic model for the same simple two-step oxidation (Mechanism 1) with no assumed RDS, then numerically calculate the macro-kinetic observables and DRCs for all species. Afterward, we compare the result of applying the DRC equations derived in *Section 2* to determining the kinetic observables with the direct simulation method in order to illustrate the robustness of the DRC equations derived in this work.

For *Section 3.1* Mechanism 1, the rate of change of the coverage of I can be written and set equal to 0 by applying the pseudo-steady state approximation [27]:

$$\frac{d\theta_I}{dt} = k_{1,f}a_R\theta_* - k_{1,r}\theta_I - k_{2,f}\theta_I + k_{2,r}a_O\theta_* = 0 \tag{52}$$

with the corresponding site balance: $\theta_* = 1 - \theta_I$. Rate constants and equilibrium constants for each step are written in the same form as before (Eqs. (29) and (32)) and the algebraic equation describing the steady-state coverage of I is then solved by applying a Newton root-finding algorithm using the Julia *NLsolve* library. For all cases in this section, the conditions are set to $a_R = 1$, $a_O = 1e^{-5}$, and $T = 298.15K$. We consider two hypothetical electrocatalysts with the energetic parameters summarized in Table 1. Case 1 gives the first reaction step a lower sensitivity to potential than the second, with electrochemical symmetry factors of $\beta_1 = 0.3$ and $\beta_2 = 0.7$. The values (and thus the potential sensitivities) are reversed for the second scenario. These parameters are chosen (within reasonable physical ranges) such that in each case, the transition state with the highest DRC changes as the potential is increased. For Case 1, the species with the highest DRC shifts from *TS*2 to *TS*1 as the applied potential is increased, primarily due to the fact that $\beta_1 < \beta_2$. The standard-state Gibbs free energy diagram corresponding to this case is shown in Fig. 1 **(a)**, where it can be seen that the barrier of step 2 is more strongly affected by increasing the applied potential than the barrier for step 1. Fig. 1**(b)** shows the DRC of each species in the mechanism as a function of the applied overpotential (using equilibrium as the reference potential). The range of potentials shown are chosen in order to operate where the reaction is far from equilibrium for ease of comparison to the analytical results from *Section 3.1*. At low potentials, *TS*2 has a DRC of 1, I has a DRC of -1, and the other species have DRCs equal to 0. Under these conditions, the forward rate could be enhanced by either lowering the Gibbs free energy of (i.e stabilizing) *TS*2 or increasing the Gibbs free energy of (i.e destabilizing) the adsorbed intermediate, I. At higher potentials, the trend shifts, such that *TS*2 and I no longer have appreciable DRCs, while *TS*1 adopts a DRC of 1.

Fig. 1**(c)** shows the explicitly-simulated (i.e. evaluated by computing the rate at a series of potentials and approximating $\frac{RT}{F}\frac{\partial \ln(r)}{\partial E}$ using finite differences) apparent transfer coefficient overlaid with the apparent transfer coefficient calculated using Eq. (12). It can be seen that the DRC equation captures the potential-dependent change in the transfer coefficient and matches the explicitly-computed value, highlighting the robustness of Eq. (12) outside of the limiting cases studied in *Section 3.1*. Similarly, Fig. 1**(d)** shows that the explicitly-simulated apparent activation energy matches the apparent activation energy predicted by Eq. (16) over the entire potential range. Finally, Fig. 1**(e)** shows that the explicitly-simulated apparent reaction order (with respect to a_R) also matches the reaction order predicted by Eq. (27). These results suggest that the DRC equations for the apparent transfer coefficient, activation energy, and reaction order capture the kinetic behavior of the system even over wide potential ranges where the DRCs of various species change appreciably.

For Case 2 in Table 1, the major differences compared to Case 1 are that this hypothetical material binds intermediate I more weakly and exhibits a smaller barrier (at the reference potential) for the second elementary step. Also in this case, $\beta_1 = 0.7$ and $\beta_2 = 0.3$, which means that the barrier for step 1 is more strongly affected by the applied potential than the barrier for step 2. This

Table 1
Energetic parameters for Case 1 and Case 2, corresponding to the simulation results in Fig. 1 and Fig. 2, respectively. These parameters are not representative of any particular material or catalyst, but are chosen to produce scenarios where the DRC of various species are illustratable as functions of potential.

	Case 1($\beta_1 = 0.3, \beta_2 = 0.7$)		Case 2($\beta_1 = 0.7, \beta_2 = 0.3$)	
Species	$H^0_{ref}(eV)$	$S^0_{ref}(eV/K)$	$H^0_{ref}(eV)$	$S^0_{ref}(eV/K)$
$R(f)$	0	0	0	0
$TS, 1(*)$	0.85	−0.0005	0.90	−0.0005
$I(*)$	−0.5	−0.001	−0.1	−0.001
$TS, 2(*)$	0.90	−0.0005	0.85	−0.0005
$O(f)$	0	0	0	0

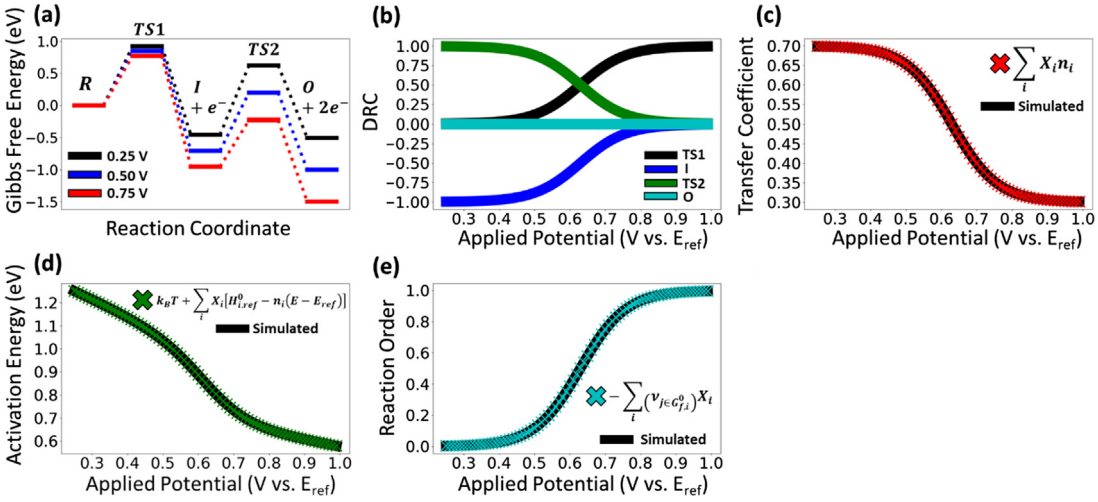

Fig. 1. **(a)** Gibbs free energy diagram corresponding to the energetics in Table 1 (Case 1) **(b)** DRC of each species **(c)** Simulated and DRC-predicted apparent transfer coefficient **(d)** Simulated and DRC-predicted apparent activation energy **(e)** Simulated and DRC-predicted apparent reaction order with respect to a_R

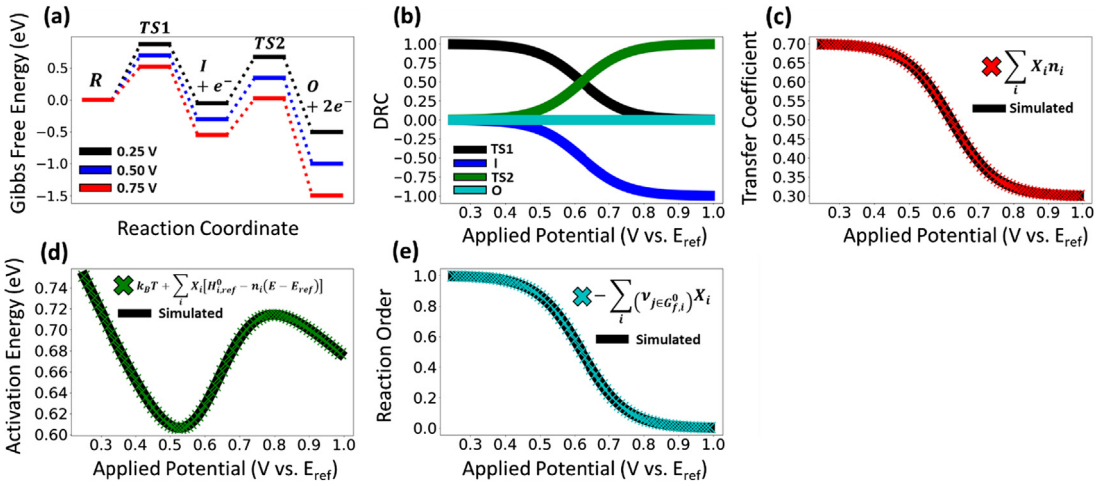

Fig. 2. **(a)** Gibbs free energy diagram corresponding to the energetics in Table 1 (Case 2) **(b)** DRC of each species **(c)** Simulated and DRC-predicted apparent transfer coefficient **(d)** Simulated and DRC-predicted apparent activation energy **(e)** Simulated and DRC-predicted apparent reaction order with respect to a_R

is clearly shown in the Gibbs free energy diagram in Fig. 2**(a)**. These parameters produce the results shown in Fig. 2**(b)**, where it can be seen that the transition state with the highest DRC shifts from *TS*1 to *TS*2 as the potential is increased. It may also be observed that the DRC of intermediate *I* shifts from 0 to −1 as the potential is increased, which is opposite to the trend observed for Case 1. This is due to the steady-state coverage of *I* increasing as the potential is increased. As was shown for Case 1, the DRC-calculated apparent transfer coefficient (Fig. 2**(c)**), activation energy (Fig. 2**(d)**), and reaction orders (Fig. 2**(e)**) all match the values that were explicitly calculated by a full simulation of the microkinetic model. Interestingly, Case 1 and Case 2 show qualitatively different behavior for the apparent activation energy as a function of potential. For Case 1, the apparent activation energy is monotonically decreasing as potential is increased, while for Case 2 it switches from decreasing to increasing between 0.5 and 0.8 V, before decreasing again. This is due to the increase in the coverage of I^* that occurs over the middle potential range, which introduces a competing effect with the barrier decreasing versus overpotential.

3.3. Case study: CO electro-oxidation

Next, we apply the relations between the DRC and the various macro-kinetic observables (transfer coefficient, activation energy, and reaction order) to analyze a model reaction of practical relevance, namely the CO electro-oxidation reaction under alkaline conditions. We consider the following steps (Mechanism 2):

$$CO(aq) + (*) \leftrightarrow CO(*) \quad \text{(M2.1)}$$
$$OH^-(aq) + (*) \leftrightarrow OH(*) + e^- \quad \text{(M2.2)}$$
$$CO(*) + OH(*) \leftrightarrow COOH(*) + (*) \quad \text{(M.2.3)}$$
$$COOH(*) + OH^-(aq) \leftrightarrow CO_2(aq) + (*) + H_2O(l) + e^- \quad \text{(M2.4)}$$

corresponding to the overall reaction $CO(aq) + 2OH^-(aq) \leftrightarrow CO_2(aq) + H_2O(l) + 2e^-$. We use the overall reaction equilibrium potential as the reference and assign a set of arbitrary, but physically realistic, standard enthalpies and entropies for the intermediates to parameterize the model, shown in Table 2. Therefore, the kinetic predictions are not necessarily representative of a particular catalyst, but are instead used to illustrate that the DRC equations derived in this work will match explicit calculations for a complex mechanism—in this case, one with parallel paths that converge in a coupling step. A free energy diagram corresponding to the parameters in Table 2 is shown in Fig. 3**(a)**. The net rate of the forward reaction is written according to the mean-field approximation [28]:

$$r_n = k_{f,n} \prod_{j \in a_{IS}} a_j \prod_{j \in \theta_{IS}} \theta_j - k_{r,n} \prod_{j \in a_{FS}} a_j \prod_{j \in \theta_{FS}} \theta_j \quad (53)$$

where r_n is the forward rate of the n^{th} elementary step, $k_{f,n}$ and $k_{r,n}$ are the forward and reverse rate constants of the n^{th} elementary step, a_j are the activities of the j^{th} species in the initial state or final state of the n^{th} step, and θ_j are the coverages in the initial state or final state of the n^{th} step. Using the pseudo-steady state approximation, the rate of change of each surface intermediate can be written as:

$$\frac{d\theta_j}{dt} = \sum_{n \in r_{FS}} \nu_n r_n - \sum_{n \in r_{IS}} \nu_n r_n = 0 \quad (54)$$

where ν_n is the stoichiometric coefficient of the j^{th} intermediate in elementary step n. The activities of all species are set to the following: $a_{CO} = 1$, $a_{OH^-} = 0.1$, $a_{CO_2} = 1e^{-5}$, and $a_{H_2O} = 1$, while the

Table 2
Energetic parameters for the CO electro-oxidation model outlined in Mechanism 2. The electrochemical adsorption of OH^- is treated as barrierless, making the deprotonation of $COOH(*)$ by OH^- the only activated electrochemical step which is assigned a symmetry factor of $\beta = 0.5$.

Species	$H^0_{ref}(eV)$	$S^0_{ref}(eV/K)$	$\nu_{CO(aq) \in G^0_{f,i}}$	$\nu_{OH^-(aq) \in G^0_{f,i}}$
$CO(aq)$	0	0	N/A	N/A
$CO(*)$	−0.75	−0.001	−1	0
$OH^-(aq)$	0	0	N/A	N/A
$OH(*)$	−0.35	−0.001	0	−1
$CO(*)\cdots OH(*)TS$	−0.4	−0.002	−1	−1
$COOH(*)$	−0.65	−0.002	−1	−1
$COOH(*)\cdots OH^-(aq)TS$	−0.55	−0.002	−1	−1
$CO_2(aq)$	0	0	−1	−1
$H_2O(l)$	0	0	0	−1

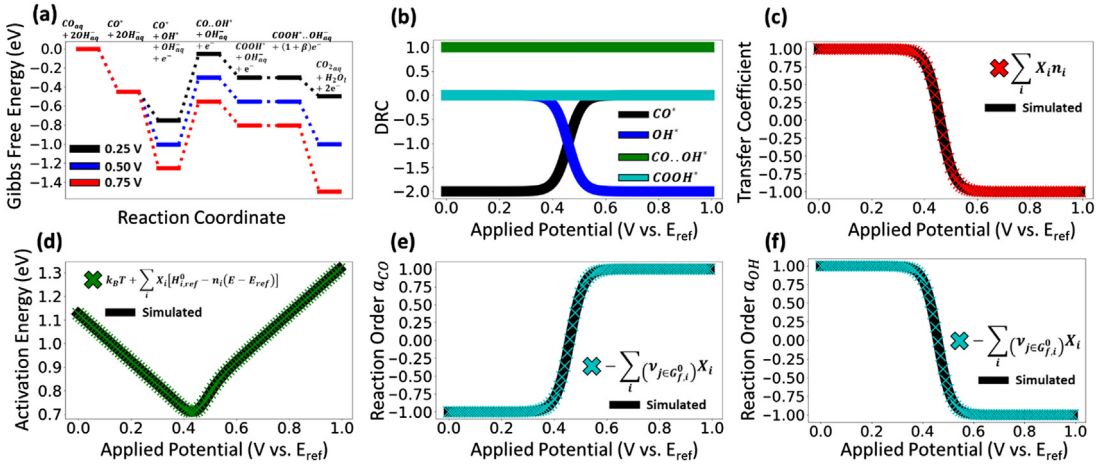

Fig. 3. **(a)** Gibbs free energy diagram at $T = 298.15K$ corresponding to the energetics listed in Table 2 at a series of applied potentials **(b)** DRC of each species **(c)** Simulated and DRC-predicted apparent transfer coefficient **(d)** Simulated and DRC-predicted apparent activation energy **(e)** Simulated and DRC-predicted apparent reaction order (with respect to a_{CO}) **(f)** Simulated and DRC-predicted apparent reaction order (with respect a_{OH^-}).

temperature is set to $T = 298.15K$. The results of the analysis are presented in Fig. 3. Fig. 3**(b)** shows the DRCs of each of the species in the mechanism, except for $COOH^* \cdots OH^-_{(aq)}$, $CO_{2(aq)}$, and $H_2O_{(l)}$, which each have DRC equal to zero at all potentials and are therefore excluded from the plot for readability. It can be seen that the $CO^* \cdots OH^*$ transition state has a DRC of 1 at all potentials, as it is the sole rate-determining transition state in the mechanism. The DRC of the CO^* adsorbate shifts from -2 at low potentials to 0 at higher potentials, which comes from the θ_{CO^*} changing from 1 to 0 over that potential range. Similarly, the DRC of the OH^* adsorbate shifts from 0 to -2 as the potential is increased due to its increasing coverage from 0 to 1 over the potential range. Fig. 3**(c)** shows the apparent transfer coefficient, which shifts from 1 to -1 as the potential is increased, with the major change occurring when the DRCs (and therefore the coverages) of the CO^* and OH^* adsorbates change their values over the 0.4–0.6 V potential range. The negative transfer coefficients can be understood in terms of a decrease in rate at high potential, which is caused by an overpopulation of OH^* electrochemically driven onto the surface; the values predicted by Eq. (12) match the explicitly-calculated transfer coefficients over the entire potential range. Fig. 3**(d)** shows the apparent activation energy, which decreases when θ_{CO^*} is high (the 0 to 0.4 V range) and then increases when θ_{OH^*} is high (0.6 to 1.0 V range). Prediction by the DRC formula (Eq. (16)) again matches the explicitly-computed values at all potentials. Finally, Fig. 3**(e)** and **(f)** show the apparent reaction orders with respect to CO_{aq} and OH^-_{aq}. $\delta_{CO_{aq}}$ takes on a value of -1 when θ_{CO^*} saturates, and similarly $\delta_{OH^-_{aq}}$ equals -1 when θ_{OH^*} saturates. Both $\delta_{CO_{aq}}$ and $\delta_{OH^-_{aq}}$ approach unity when the coverages of CO^* and OH^* are close to 0, respectively. The reaction orders predicted by Eq. (27) indeed also match those explicitly determined from the solution of the microkinetic model. The above analysis further illustrates the reliability of the DRC expressions derived in this work to predict the macro-kinetic observables for a wide variety of electrocatalytic reactions.

3.4. Secondary effects

3.4.1. Electric field effects

In the derivation of the macro-kinetic observables in Section 2, it was assumed that the effect of the applied potential on the free energy of a given species was solely due to the electrons transferred to form that species. However, in many cases the standard enthalpy and entropy of chemical intermediates can also be potential-dependent. One way this can be manifested is through electric field effects, which can change the binding enthalpy of adsorbates due to their surface dipole moment and polarizability [29]. This will be accounted in pure electrostatic terms, neglecting additional small shifts, for example by changing vibrational frequency, that would also slightly affect entropy. Reproducing Eq. (9), the Gibbs free energy of species i at a given potential is:

$$G_i^0 = H_{i,ref}^0 - TS_{i,ref}^0 + \left(H_i^0 - H_{i,ref}^0\right) - T\left(S_i^0 - S_{i,ref}^0\right) - n_i F\left(E - E_{ref}\right) \tag{55}$$

Now, H_i^0 is a function of the changing electric field as the potential is varied. The strength of the electric field at the electrode–electrolyte interface is approximately proportional to the difference between the potential-of-zero-charge (pzc) and the operating potential [30–35], permitting the expression:

$$H_i^0 = H_{i,pzc}^0 + \Delta H_{i,EF}^0 \tag{56}$$

where $H_{i,pzc}^0$ is the standard enthalpy of species i at the pzc (i.e. in the absence of an electric field) and $\Delta H_{i,EF}^0$ is the change in the standard enthalpy of species i due to the electric field. If we estimate the thickness of the double layer to be ~ 1Å and assume that the entire potential drop occurs roughly linearly over this region, then we may further write (for surface-adsorbed intermediates):

$$\Delta H_{i,EF}^0 = -\mu_{0,i}\left(E - E_{pzc}\right) - \frac{1}{2}p_i\left(E - E_{pzc}\right)^2 \tag{57}$$

where $\mu_{0,i}$ is the adsorbate dipole moment in eÅ and p_i is the polarizability in $e\text{Å}^2V^{-2}$ [36]. After incorporating this into the total Gibbs free energy of species i, simplifying, and keeping the entropy term constant (i.e. $S_i^0 = S_{i,ref}^0$ at all potentials), we may write:

$$G_i^0 = \left(H_{i,pzc}^0 - \mu_{0,i}\left(E - E_{pzc}\right) - \frac{1}{2}p_i\left(E - E_{pzc}\right)^2\right) - TS_{i,ref}^0 - n_i F\left(E - E_{ref}\right) \tag{58}$$

The DRC equation for the apparent transfer coefficient can then be adapted to account for these electric field effects:

$$\begin{aligned}\alpha &= \frac{RT}{F}\left[\sum_i X_i \frac{\partial\left[\frac{-\left(H_{i,pzc}^0 - \mu_{0,i}\left(E-E_{pzc}\right) - \frac{1}{2}p_i\left(E-E_{pzc}\right)^2\right)}{RT} + \frac{S_{i,ref}^0}{R} + \frac{n_i F\left(E-E_{ref}\right)}{RT}\right]}{\partial E}\right] \\ &= \frac{RT}{F}\sum_i X_i\left[\mu_{0,i} + p_i\left(E - E_{pzc}\right) + n_i\right]\end{aligned} \tag{59}$$

Similarly, the apparent activation energy can be written as:

$$E_{app} = k_B T + \left[\sum_i X_i \left(H^0_{i,pzc} - \mu_{0,i}(E - E_{pzc}) - \frac{1}{2}p_i(E - E_{pzc})^2 - n_i(E - E_{ref})\right)\right] \quad (60)$$

The apparent reaction order equation remains unaffected since it contains no explicit dependence on the standard enthalpies of the species in the mechanism outside of the DRC terms themselves.

We can now examine how the field effects produce deviations from the idealized behavior for the simple two-step oxidation mechanism from Section 3.2 (specifically, using the "Case 1" energetic parameters). We assign the intermediate I^* physically reasonable values of $\mu_{0,I} = -0.133 e\text{Å}$ and $p_I = 0.083 e\text{Å}^2 V^{-2}$ (calculated by others to be representative of the CO* adsorbate on Pt (1 1 1) [36]), and also assume that the pzc is identical to the reference potential on this hypothetical material for simplicity. Fig. 4**(a–c)** shows the transfer coefficient, apparent activation energy, and apparent reaction order for both the idealized case (black lines - simulated, red markers – DRC equations) and the case with electric field effects (blue lines - simulated, yellow markers – DRC equations). It can be seen that all three observables deviate in a somewhat significant manner from the ideal scenario when these secondary effects are accounted. In this particular example, the I^* adsorbate's binding enthalpy is weakened due to the electric field as the potential is increased, which has the effect of decreasing the apparent activation energy relative to the ideal case. Indeed, the ideal and non-ideal cases match at high potentials where θ_{I^*} is low and therefore the binding energy of $I^*$is inconsequential to the rate of reaction. However, we note that for all observables, for both the ideal and non-ideal cases, the predictions of the DRC equations derived in this work match exactly the explicitly calculated parameters, indicating that the DRC expressions can be modified as shown in Eqs. (59) and (60) to capture electric field effects.

It is important to also note that the electric field can have many other effects, for example in the ordering of interfacial solvent molecules. In aqueous systems, interfacial water may adopt preferential orientations depending on the strength and direction of the electric field [37], which has been shown, for example, to affect the pH-dependent kinetics of the hydrogen evolution reaction [31,35]. Near the pzc, the interfacial water adopts a configuration of "maximum entropy" since there is no field imposing an orientation [38]. These configurational influences will not only affect the reorganization energy of electron transfers but also change the extent to which water stabilizes various chemical species through hydrogen bonding [39]. A further implication is that solvation energies of adsorbates are not expected to be constant across different materials, since their work functions and thus pzc's can vary and lead to different electric field strengths at a given applied potential. Given these considerations, it is clear that there does not yet exist a general quantitative description of how the potential is expected to change the Gibbs free energy of the chemical intermediates in the mechanism—especially those interacting strongly with solvent. Naturally, further effects can be built in to the framework here with additional energy terms and appropriate parameterization, and more accurate modeling might be achieved by the use of free energies directly calculated by *ab initio* approaches, for which grand canonical (fixed potential) simulations and large scale molecular dynamics for solvation are becoming more accessible [20,40,41]. The examples here and in the following section simply serve to illustrate the general approach to incorporating these effects and the degree to which a subset of realistic nonidealities can cause deviations from the predictions of basic mechanistic models.

3.4.2. Potential-dependent symmetry factors

We next consider the fact that the symmetry factor of an elementary charge-transfer step can be potential-dependent. This largely relates to the transition state becoming earlier or later with respect to changing potential and can still be interpreted in terms of an extent of partial charge transfer at the transition state. To capture the potential-dependence, we may write a linear approximation for the number of electrons transferred to reach the state as:

$$n_i = n_{i,ref} + \gamma_{i,e^-}(E - E_{ref}) \quad (61)$$

where γ_{i,e^-} is a linear scaling parameter capturing the extent to which the elementary symmetry factor changes with the applied potential. Marcus theory is an example of a model which predicts a symmetry factor that is a linear function of the applied overpotential; in the simplest version it suggests the form [42]:

$$\beta_i = \frac{1}{2} + \frac{F\eta_i}{2\lambda_i} \quad (62)$$

where λ_i is the solvent reorganization energy (usually up to a few eV) corresponding to the elementary step forming transition state i, and η_i is the overpotential with respect to the equilibrium of that step. In this case, the linear scaling parameter is:

$$\gamma_{i,e^-} = \frac{F}{2\lambda_i} \quad (63)$$

While the linearity only strictly applies to outer-sphere electron transfers and can in particular deviate under large electronic overlap and hybridization between intermediates and the electrode [43], Eq. (63) provides a means to estimate a reasonable magnitude for γ_{i,e^-}. We also note that the linear scaling parameter is equal to

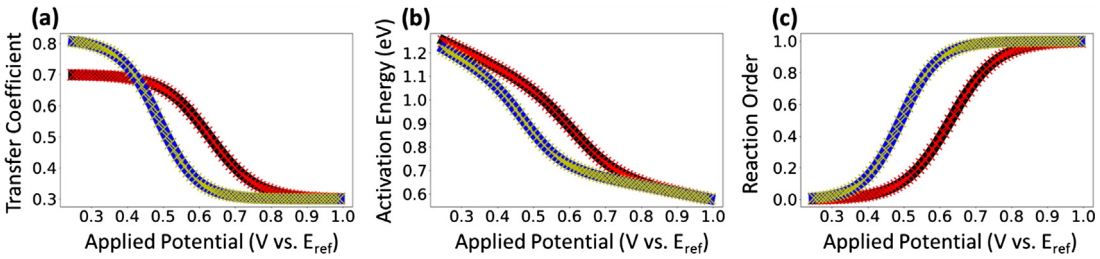

Fig. 4. **(a)** Apparent transfer coefficient **(b)** apparent activation energy and **(c)** apparent reaction order for Mechanism 1 (*Section 3.2*) for both the idealized case (explicit values – black line, DRC-calculated values – red "x" markers) and the case of electric field effects as described in *Section 3.4.1* (explicit values – blue line, DRC-calculated values – yellow "x" markers). The dipole moment of the intermediate "I" was set to −0.133 *e*Å, the polarizability to 0.083 $e\text{Å}^2 V^{-2}$ and the pzc was set to the reference potential. All other parameters match the "Case 1" energetics from Table 1. (For interpretation of the references to colour in this figure legend, the reader is referred to the web version of this article.)

zero for intermediates with integer n_i in their respective formation energies, as only transition states are associated with a symmetry factor.

Incorporating potential-dependent symmetry factors into the total Gibbs free energy of each species, and assuming that no other nonidealities are present, we may write:

$$G_i^0 = H_{i,ref}^0 - TS_{i,ref}^0 - \left(n_{i,ref} + \gamma_{i,e^-}(E - E_{ref})\right)F(E - E_{ref}) \tag{64}$$

The adapted equation for the apparent transfer coefficient is then written as:

$$\alpha = \frac{RT}{F}\left[\sum_i X_i \frac{\partial\left[\frac{-H_{i,ref}^0}{RT} + \frac{S_{i,ref}^0}{R} + \frac{\left(n_{i,ref} + \gamma_{i,e^-}(E - E_{ref})\right)F(E - E_{ref})}{RT}\right]}{\partial E}\right]$$
$$= \frac{RT}{F}\sum_i X_i\left[n_{i,ref} + 2\gamma_{i,e^-}(E - E_{ref})\right] \tag{65}$$

while the apparent activation energy can be written in the following way:

$$E_{app} = k_BT + \sum_i X_i\left[H_{i,ref}^0 - \left(n_{i,ref} + \gamma_{i,e^-}(E - E_{ref})\right)(E - E_{ref})\right] \tag{66}$$

To demonstrate the impact of potential-dependent symmetry factors, we consider again the simple two-step oxidation mechanism from *Section 3.2* using the energetics outlined as Case 1 in Table 1. Fig. 5 **(a-c)** similarly show all three macro-kinetic observables for the ideal case, as well as the case where the barriers for both steps are treated as having potential-dependent symmetry factors according to Eq. (61). We choose a value of $\gamma_{e^-} = 0.166$ for both of the elementary step transition states, which would correspond to a reorganization energy of 3 eV, reasonable for electrode adsorption/desorption processes [44]. Both the transfer coefficient and the apparent activation energy deviate noticeably from the ideal cases, while the apparent reaction orders with respect to a_R are identical (they perfectly overlap each other which makes only one set of markers visible). The reason why the reaction order remains unaffected relative to the ideal case is due to the fact that both *TS*1 and *TS*2 were made "equally non-ideal", yielding the same balance in the coverage of I^* as in the ideal case. Ultimately the example shows that the DRC equations again are valid for predicting all of the explicit macro-kinetic observables.

3.4.3. Adsorbate-adsorbate interactions

Finally, perhaps the most universal nonideality across all areas of surface kinetics can come from changes to the adsorption energy of a given species, induced by the coverages of adsorbates on the surface. A Frumkin adsorption isotherm is one estimation of this effect, which approximates the standard Gibbs free energy of a single intermediate as a function of that intermediate's coverage (at a given potential) as:

$$G_i^0 = G_{i,\theta_i=0}^0 + z_i\theta_i \tag{67}$$

where z_i is an interaction parameter specific to species i more generally written as $z_i = \left(\frac{dG_i^0}{d\theta_i}\right)$. Positive and negative values represent repulsive and attractive interactions, respectively. The coverage-dependent equilibrium constant associated with adsorption of an intermediate i obeying a Frumkin-type isotherm can then be expressed as:

$$K(\theta_i) = \exp\left(\frac{-\left(\Delta G_i^0 + z_i\theta_i\right)}{k_BT}\right) = K_{\theta_i=0}\exp\left(\frac{-z_i\theta_i}{k_BT}\right) \tag{68}$$

where $K_{\theta_i=0}$ is the equilibrium constant in the limit of zero coverage of "i". We once again apply nonideality, here through a Frumkin-type isotherm for I^*, to the simple two-step oxidation mechanism with the energetics outlined as Case 1 in Table 1. This yields the following corrections to the desorption rate constants associated with intermediate I^* (while the non-adsorbed species are unaffected):

$$k_{1,r}(\theta_I) = k_{1,r,\theta_I=0}\exp\left(\frac{z_I\theta_I}{k_BT}\right) \tag{69}$$

$$k_{2,f}(\theta_I) = k_{2,f,\theta_I=0}\exp\left(\frac{z_I\theta_I}{k_BT}\right) \tag{70}$$

Since both the apparent reaction order and apparent transfer coefficient are functions only of the DRCs of the various species in the mechanism and the number of electrons in a given state, the only macro-kinetic observable requiring an explicit adjustment in its written form is the apparent activation energy, which becomes:

$$E_{app} = k_BT + \sum_i X_i\left[(H_{i,ref}^0 + z_i\theta_i) - n_i(E - E_{ref})\right] \tag{71}$$

which accounts for the effect of the coverage on the standard-state enthalpy of a given species. Fig. 6 shows examples of the three macro-kinetic observables for a few different cases of repulsive interactions among species I^*. As the interaction parameter increases in magnitude, each of the observables begins to deviate significantly from its respective low coverage limiting behavior. As expected, imposing repulsive interactions to the I^* intermediate results in a decrease in the apparent transfer coefficient and apparent activation energy at potentials where θ_{I^*} is significant (while the apparent reaction order with respect to $R(f)$ increases due to a mitigation of the inhibitory effects of I^*). At high potentials where θ_{I^*} is low, the ideal and nonideal cases are identical since I^* has a low DRC under those conditions. However, in all cases the DRC-predicted values again match exactly the explicitly-simulated

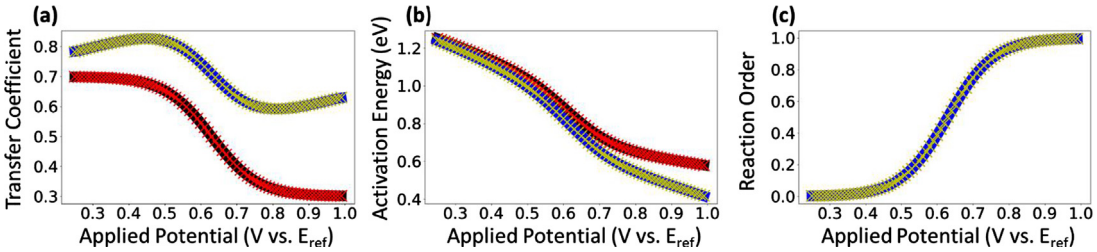

Fig. 5. **(a)** Apparent transfer coefficient **(b)** apparent activation energy and **(c)** apparent reaction order for Mechanism 1 for both the idealized case (explicit values – black line, DRC-calculated values – red "x" markers) and the case of potential dependent symmetry factors (explicit values – blue line, DRC-calculated values – yellow "x" markers). All parameters were assumed to be ideal except the linear partial charge transfer scaling parameter, γ_{e^-}, set to 0.166 for both TS1 and TS2, corresponding to a reorganization energy of 3 eV. All other model parameters are identical to "Case 1" from Table 1. (For interpretation of the references to colour in this figure legend, the reader is referred to the web version of this article.)

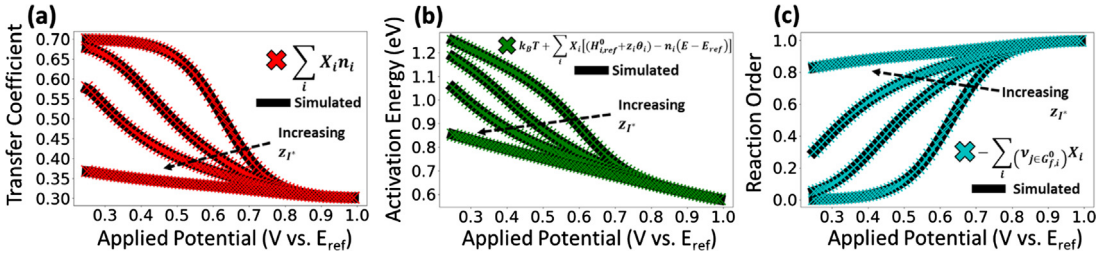

Fig. 6. (**a**) Apparent transfer coefficient (**b**) apparent activation energy and (**c**) apparent reaction order for Mechanism 1 with varying values of the Frumkin interaction parameter z_I. All energetic parameters other than the Frumkin correction parameter correspond to "Case 1" from Table 1. The four values of z_I shown above are, in increasing order, [0, 0.05, 0.10, 0.25].

values. Therefore, we conclude that, while accounting for adsorbate–adsorbate interactions may be necessary to correctly capture the behavior of electrocatalytic systems that operate at high coverages, the DRC equations can still apply to these cases incorporating only the small change made in the description of the apparent activation energy above.

4. Conclusions

The equations derived herein provide simple descriptions of various macro-kinetic observables in terms of the DRCs of each of the species in an electrocatalytic mechanism. Since the thermodynamic DRCs of reaction intermediates can be directly related to their surface coverages, these expressions can provide a direct link between the macro-kinetic behavior of a reacting system (Tafel slopes, activation energies, and reaction orders) and microkinetic quantities which can also be experimentally interrogated (e.g. coverages). It is worth noting that experimental coverages can also be used to infer the likely transition states with high DRCs – for example, high-coverage intermediates are typically followed, as opposed to preceded, by high-DRC transition states in a given pathway. Moreover, since it is typical that only a few species in the mechanism have non-negligible DRCs, these expressions can greatly simplify the process of formulating hypotheses about reaction mechanisms and comparing the resultant predictions to experiment. It is interesting to note that each of these macro-kinetic observables are also correlated in a well-defined way, in the sense that they each depend on a common set of variables which are the DRCs of each of the species in the mechanism. Considering both the inherent complexities of multistep mechanisms as well as possibilities of significant nonidealities, we advocate that a holistic approach should be taken to identify likely mechanisms of electrochemical processes, specifically incorporating reaction data across a wide range of potentials, temperatures, and reactant activities in order to compare to the predictions of microkinetic models using the equations derived in this work.

Declaration of Competing Interest

The authors declare that they have no known competing financial interests or personal relationships that could have appeared to influence the work reported in this paper.

Acknowledgements

The authors acknowledge support from the National Science Foundation (CBET 1944834). A.A.B acknowledges support from the DoED GAANN fellowship. We would also like to thank Charlie Campbell and Zhongtian Mao for a careful reading of the manuscript.

Appendix A. Supplementary material

Supplementary data to this article can be found online at https://doi.org/10.1016/j.jcat.2021.03.014.

References

[1] A.J. Bard, L.R. Faulkner, Electrochemical Methods: Fundamentals and Applications, John Wiley & Sons Inc, Second, 2001.
[2] Y. Fang, Z. Liu, Tafel Kinetics of Electrocatalytic Reactions : From Experiment to First- Principles, (2014). https://doi.org/10.1021/cs501312v.
[3] M.T.M. Koper, Theory of multiple proton–electron transfer reactions and its implications for electrocatalysis, Chem. Sci. 4 (2013) 2710, https://doi.org/10.1039/c3sc50205h.
[4] A. Holewinski, S. Linic, Elementary Mechanisms in Electrocatalysis: Revisiting the ORR Tafel Slope, J. Electrochem. Soc. 159 (2012) H864–H870, https://doi.org/10.1149/2.022211jes.
[5] T. Shinagawa, A.T. Garcia-Esparza, K. Takanabe, Insight on Tafel slopes from a microkinetic analysis of aqueous electrocatalysis for energy conversion, Sci. Rep. 5 (2015) 1–21, https://doi.org/10.1038/srep13801.
[6] B.V. Tilak, B.E. Conway, Analytical Relations Between Reaction Order and Tafel Slope Derivatives For Electrocatalytic Reactions Involving Chemisorbed Intermediates, Electrochim. Acta. 37 (1992) 51–61.
[7] B.E. Conway, L. Bai, M.A. Sattar, Role of the transfer coefficient in electrocatalysis: Applications to the H2 and O2 evolution reactions and the characterization of participating adsorbed intermediates, Int. J. Hydrogen Energy. 12 (1987) 607–621, https://doi.org/10.1016/0360-3199(87)90002-4.
[8] J.T. Mefford, Z. Zhao, M. Bajdich, W.C. Chueh, Interpreting Tafel behavior of consecutive electrochemical reactions through combined thermodynamic and steady state microkinetic approaches, Energy Environ. Sci. 13 (2020) 622–634, https://doi.org/10.1039/c9ee02697e.
[9] A. Govind Rajan, E.A. Carter, Microkinetic model for pH- and potential-dependent oxygen evolution during water splitting on Fe-doped β-NiOOH, Energy Environ. Sci. 13 (2020) 4962–4976, https://doi.org/10.1039/d0ee02292f.
[10] A.T. Marshall, Using microkinetic models to understand electrocatalytic reactions, Curr. Opin. Electrochem. 7 (2018) 75–80, https://doi.org/10.1016/j.coelec.2017.10.024.
[11] P.S. Lamoureux, A.R. Singh, K. Chan, pH Effects on Hydrogen Evolution and Oxidation over Pt(111): Insights from First-Principles, ACS Catal. 9 (2019) 6194–6201, https://doi.org/10.1021/acscatal.9b00268.
[12] R. Guidelli, R.G. Compton, J.M. Feliu, E. Gileadi, J. Lipkowski, W. Schmickler, S. Trasatti, Defining the transfer coefficient in electrochemistry: An assessment (IUPAC Technical Report), Pure Appl. Chem. 86 (2014) 245–258, https://doi.org/10.1515/pac-2014-5026.
[13] J.O'.M. Bockris, Z. Nagy, Symmetry factor and transfer coefficient. A source of confusion in electrode kinetics, J. Chem. Educ. 50 (1973) 839, https://doi.org/10.1021/ed050p839.
[14] C.T. Campbell, The Degree of Rate Control : A Powerful Tool for Catalysis Research, ACS Catal. 7 (2017) 2770–2779, https://doi.org/10.1021/acscatal.7b00115.
[15] C. Stegelmann, A. Andreasen, C.T. Campbell, Degree of rate control: How much the energies of intermediates and transition states control Rates (Journal of the American Chemical Society (2009), 131, (8077–8082)), J. Am. Chem. Soc. 131 (2009) 13563, https://doi.org/10.1021/ja9065199.
[16] M. Jørgensen, H. Grönbeck, Connection between macroscopic kinetic measurables and the degree of rate control, Catal. Sci. Technol. 7 (2017) 4034–4040, https://doi.org/10.1039/c7cy01246b.
[17] Z. Mao, C.T. Campbell, Apparent Activation Energies in Complex Reaction Mechanisms: A Simple Relationship via Degrees of Rate Control, ACS Catal. 9 (2019) 9465–9473, https://doi.org/10.1021/acscatal.9b02761.
[18] B.L. Foley, A. Bhan, Degree of rate control and De Donder relations – An interpretation based on transition state theory, J. Catal. 384 (2020) 231–251, https://doi.org/10.1016/j.jcat.2020.02.008.

[19] Z. Mao, C.T. Campbell, The degree of rate control of catalyst-bound intermediates in catalytic reaction mechanisms: Relationship to site coverage, J. Catal. 381 (2020) 53–62, https://doi.org/10.1016/j.jcat.2019.09.044.
[20] P. Lindgren, G. Kastlunger, A.A. Peterson, A Challenge to the G ~0 Interpretation of Hydrogen Evolution, ACS Catal. 10 (2020) 121–128, https://doi.org/10.1021/acscatal.9b02799.
[21] K. Chan, J.K. Norskov, Potential Dependence of Electrochemical Barriers from ab Initio Calculations, J. Phys. Chem. Lett. 7 (2016) 1686–1690, https://doi.org/10.1021/acs.jpclett.6b00382.
[22] R.A. Marcus, On the Theory of Electron-Transfer Reactions. VI. Unified Treatment for Homogeneous and Electrode Reactions, J. Chem. Phys. 43 (1965) 679–701, https://doi.org/10.1063/1.1696792.
[23] A.M. Roman, J. Dudoff, A. Baz, A. Holewinski, Identifying " Optimal " Electrocatalysts: Impact of Operating Potential and Charge Transfer Model, ACS Catal. 7 (2017) 8641–8652, https://doi.org/10.1021/acscatal.7b03235.
[24] A.J. Medford, C. Shi, M.J. Hoffmann, A.C. Lausche, S.R. Fitzgibbon, T. Bligaard, J. K. Nørskov, CatMAP: A Software Package for Descriptor-Based Microkinetic Mapping of Catalytic Trends, Catal. Lett. 145 (2015) 794–807, https://doi.org/10.1007/s10562-015-1495-6.
[25] A.H. Motagamwala, J.A. Dumesic, Microkinetic Modeling: A Tool for Rational Catalyst Design, Chem. Rev. (2020), https://doi.org/10.1021/acs.chemrev.0c00394.
[26] A.H. Motagamwala, M.R. Ball, J.A. Dumesic, Microkinetic Analysis and Scaling Relations for Catalyst Design, (2018) 1–38. https://doi.org/10.1146/annurev-chembioeng-060817-084103
[27] H. Lynggaard, A. Andreasen, C. Stegelmann, P. Stoltze, Analysis of simple kinetic models in heterogeneous catalysis, Prog. Surf. Sci. 77 (2004) 71–137, https://doi.org/10.1016/j.progsurf.2004.09.001.
[28] A.J. Medford, A.C. Lausche, F. Abild-Pedersen, B. Temel, N.C. Schjødt, J.K. Nørskov, F. Studt, Activity and selectivity trends in synthesis gas conversion to higher alcohols, Top. Catal. 57 (2014) 135–142, https://doi.org/10.1007/s11244-013-0169-0.
[29] F. Che, J.T. Gray, S. Ha, N. Kruse, S.L. Scott, J.S. McEwen, Elucidating the Roles of Electric Fields in Catalysis: A Perspective, ACS Catal. 8 (2018) 5153–5174, https://doi.org/10.1021/acscatal.7b02899.
[30] N. García-Aráez, V. Climent, J.M. Feliu, Potential-dependent water orientation on Pt(1 1 1) stepped surfaces from laser-pulsed experiments, Electrochim. Acta. 54 (2009) 966–977, https://doi.org/10.1016/j.electacta.2008.08.016.
[31] F.J. Sarabia, P. Sebastián-Pascual, M.T.M. Koper, V. Climent, J.M. Feliu, Effect of the Interfacial Water Structure on the Hydrogen Evolution Reaction on Pt(111) Modified with Different Nickel Hydroxide Coverages in Alkaline Media, ACS Appl. Mater. Interfaces. 11 (2019) 613–623, https://doi.org/10.1021/acsami.8b15003.
[32] K.I. Ataka, T. Yotsuyanagi, M. Osawa, Potential-dependent reorientation of water molecules at an electrode/electrolyte interface studied by surface-enhanced infrared absorption spectroscopy, J. Phys. Chem. 100 (1996) 10664–10672, https://doi.org/10.1021/jp953636z.
[33] A.N. Frumkin, O.A. Petrii, Potentials of zero total and zero free charge of platinum group metals, Electrochim. Acta. 20 (1975) 347–359, https://doi.org/10.1016/0013-4686(75)90017-1.
[34] E.M. Stuve, Ionization of water in interfacial electric fields: An electrochemical view, Chem. Phys. Lett. 519–520 (2012) 1–17, https://doi.org/10.1016/j.cplett.2011.09.040.
[35] I. Ledezma-Yanez, W.D.Z. Wallace, P. Sebastián-Pascual, V. Climent, J.M. Feliu, M.T.M. Koper, Interfacial water reorganization as a pH-dependent descriptor of the hydrogen evolution rate on platinum electrodes, Nat. Energy. 2 (2017) 1–7, https://doi.org/10.1038/nenergy.2017.31.
[36] M. Shetty, M. Ardagh, Y. Pang, O. Abdelrahman, P. Dauenhauer, Electric-Field Assisted Modulation of Surface Thermochemistry, (2020). https://doi.org/10.26434/chemrxiv.12127191.
[37] J. Ryu, Y. Surendranath, Tracking Electrical Fields at the Pt/H2O Interface during Hydrogen Catalysis, J. Am. Chem. Soc. 141 (2019) AR. https://doi.org/10.1021/jacs.9b05148.
[38] A.R. Zeradjanin, G. Polymeros, C. Toparli, M. Ledendecker, N. Hodnik, A. Erbe, M. Rohwerder, F. La Mantia, What is the trigger for the hydrogen evolution reaction? - Towards electrocatalysis beyond the Sabatier principle, Phys. Chem. Chem. Phys. 22 (2020) 8768–8780, https://doi.org/10.1039/d0cp01108h.
[39] H.H. Heenen, J.A. Gauthier, H.H. Kristoffersen, T. Ludwig, K. Chan, Solvation at metal/water interfaces: An ab initio molecular dynamics benchmark of common computational approaches, J. Chem. Phys. 152 (2020), https://doi.org/10.1063/1.5144912.
[40] J.D. Goodpaster, A.T. Bell, M. Head-Gordon, Identification of Possible Pathways for C-C Bond Formation during Electrochemical Reduction of CO2: New Theoretical Insights from an Improved Electrochemical Model, J. Phys. Chem. Lett. 7 (2016) 1471–1477, https://doi.org/10.1021/acs.jpclett.6b00358.
[41] H. Xiao, T. Cheng, W.A. Goddard, R. Sundararaman, Mechanistic Explanation of the pH Dependence and Onset Potentials for Hydrocarbon Products from Electrochemical Reduction of CO on Cu (111), J. Am. Chem. Soc. 138 (2016) 483–486, https://doi.org/10.1021/jacs.5b11390.
[42] R.A. Marcus, On the Theory of Oxidation-Reduction Reactions Involving Electron Transfer. I, J. Chem. Phys. 24 (1956) 966–978, https://doi.org/10.1063/1.1742723.
[43] E. Santos, P. Quaino, W. Schmickler, Theory of electrocatalysis: hydrogen evolution and more, Phys. Chem. Chem. Phys. 14 (2012) 11224, https://doi.org/10.1039/c2cp40717e.
[44] E. Santos, W. Schmickler, Electrocatalysis of hydrogen oxidation - Theoretical foundations, Angew. Chemie - Int. Ed. 46 (2007) 8262–8265, https://doi.org/10.1002/anie.200702338.